Intermodulation electrostatic force microscopy for imaging surface photo-voltage

Riccardo Borgani, Daniel Forchheimer, Jonas Bergqvist, Per-Anders Thorén, Olle Inganäs, and David B. Haviland

Citation: Applied Physics Letters **105**, 143113 (2014); doi: 10.1063/1.4897966
View online: http://dx.doi.org/10.1063/1.4897966
View Table of Contents: http://scitation.aip.org/content/aip/journal/apl/105/14?ver=pdfcov
Published by the AIP Publishing

Articles you may be interested in
High potential sensitivity in heterodyne amplitude-modulation Kelvin probe force microscopy
Appl. Phys. Lett. **100**, 223104 (2012); 10.1063/1.4723697

Half-harmonic Kelvin probe force microscopy with transfer function correction
Appl. Phys. Lett. **100**, 063118 (2012); 10.1063/1.3684274

Special cantilever geometry for the access of higher oscillation modes in atomic force microscopy
Appl. Phys. Lett. **89**, 033106 (2006); 10.1063/1.2226993

Reconstruction of electrostatic force microscopy images
Rev. Sci. Instrum. **76**, 083705 (2005); 10.1063/1.1988089

Imaging of a silicon pn junction under applied bias with scanning capacitance microscopy and Kelvin probe force microscopy
Appl. Phys. Lett. **77**, 106 (2000); 10.1063/1.126892

AIP Chaos
CALL FOR APPLICANTS
Seeking new Editor-in-Chief

This article is copyrighted as indicated in the article. Reuse of AIP content is subject to the terms at: http://scitation.aip.org/termsconditions. Downloaded to IP: 77.238.32.12
On: Tue, 14 Oct 2014 12:41:39

APPLIED PHYSICS LETTERS **105**, 143113 (2014)

Intermodulation electrostatic force microscopy for imaging surface photo-voltage

Riccardo Borgani,[1,a)] Daniel Forchheimer,[1] Jonas Bergqvist,[2] Per-Anders Thorén,[1] Olle Inganäs,[2] and David B. Haviland[1,b)]
[1]*Nanostructure Physics, Royal Institute of Technology, 10691 Stockholm, Sweden*
[2]*Department of Physics, Chemistry and Biology, Linköping University, 58183 Linköping, Sweden*

(Received 22 August 2014; accepted 30 September 2014; published online 10 October 2014)

We demonstrate an alternative to Kelvin Probe Force Microscopy for imaging surface potential. The open-loop, single-pass technique applies a low-frequency AC voltage to the atomic force microscopy tip while driving the cantilever near its resonance frequency. Frequency mixing due to the nonlinear capacitance gives intermodulation products of the two drive frequencies near the cantilever resonance, where they are measured with high signal to noise ratio. Analysis of this intermodulation response allows for quantitative reconstruction of the contact potential difference. We derive the theory of the method, validate it with numerical simulation and a control experiment, and we demonstrate its utility for fast imaging of the surface photo-voltage on an organic photovoltaic material. © *2014 AIP Publishing LLC*. [http://dx.doi.org/10.1063/1.4897966]

One of the most popular and useful methods of Electrostatic Force Microscopy (EFM) is Kelvin Probe Force Microscopy (KPFM),[1] which provides a measurement of the contact potential difference V_{CPD} (sometimes referred to as the surface potential). KPFM is widely used for advanced imaging of composite polymeric materials[2] and for imaging of the local work function on the surface of organic photovoltaic materials.[3] Although KPFM is a useful technique to investigate electric properties of surfaces at the nanoscale, the signal-to-noise ratio, accuracy, and speed are limited by the additional feed-back loops commonly used in its implementations.[4] To overcome these limitations, an open-loop technique was first proposed by Takeuchi *et al*.[5] to image the contact potential difference in vacuum. Later, the technique was used to measure the potential of nanoparticles in liquid[6] and to characterise ferroelectric thin films.[7]

In this paper, we propose and demonstrate an open-loop technique that exploits the intermodulation (frequency mixing) of an electrostatic drive force and a mechanical drive force, to up-convert the electrostatic frequency to the first flexural resonance where the high quality factor allows for a more sensitive measurement. The contact potential difference can be imaged in a single-pass, allowing for imaging times shorter than 5 min with 256×256 pixel resolution.

The electrostatic energy stored in a system of two perfect conductors is $E_{\text{EL}} = \frac{1}{2}CV^2$, where C is the capacitance and V the electrostatic potential difference between the two. The attractive electrostatic force is therefore

$$F_{\text{EL}} = \frac{1}{2}\frac{\partial C}{\partial z}V^2, \tag{1}$$

where z is the distance between the two conductors. In EFM, the two conductors are the conductive tip and the sample substrate, which can be approximated as an axially symmetric electrode and an infinite conducting plane, respectively. The resulting capacitance gradient varies as a non-linear function of z that depends on the tip geometry.[8]

Intermodulation EFM (ImEFM) excites the cantilever with a shaker piezo at frequency ω_{D} close to resonance ω_0, while at the same time an AC voltage is applied to the cantilever at frequency $\omega_{\text{E}} \ll \omega_{\text{D}}$. The total potential between the tip and the sample is

$$V(t) = V_{\text{CPD}} + V_{\text{AC}}\cos(\omega_{\text{E}}t + \phi_{\text{E}}), \tag{2}$$

where V_{CPD} is the contact potential difference between the tip and the sample, assumed to be function of the in-plane tip position, and ϕ_{E} is an arbitrary phase delay between the applied voltage and the lock-in reference signal. For a high Q cantilever oscillation, the tip motion is dominantly harmonic at $\omega_{\text{D}} \approx \omega_0$. The time evolution of the tip-sample distance may be written,

$$z(t) \approx h + A_{\text{D}}\cos(\omega_{\text{D}}t + \phi_{\text{D}}), \tag{3}$$

where h is the tip rest position (or static probe height), and A_{D} and ϕ_{D} are the oscillation amplitude and phase, which depend on the drive force and on the interaction with the surface.

The capacitance gradient is a non-linear function of the tip-sample separation z. We define $C' = \frac{\partial C}{\partial z}$ and perform a polynomial expansion around the resting position h

$$C'(z) = \sum_{n=0}^{+\infty}\frac{1}{n!}\left.\frac{\partial^n C'}{\partial z^n}\right|_h (z-h)^n, \tag{4}$$

which together with Eq. (3) gives

$$\begin{aligned} C'(t) &= \sum_{n=0}^{+\infty}\frac{A_{\text{D}}^n}{n!}\left.\frac{\partial^n C'}{\partial z^n}\right|_h \cos^n(\omega_{\text{D}}t + \phi_{\text{D}}) \\ &= \sum_{k=0}^{+\infty} a_k\cos(k\omega_{\text{D}}t + k\phi_{\text{D}}), \end{aligned} \tag{5}$$

where the coefficients a_k are linear combinations of the terms $C'^{(n)}A_{\text{D}}^n/n!$. Inserting Eqs. (2) and (5) into Eq. (1) gives

a)Electronic mail: borgani@kth.se
b)Electronic mail: haviland@kth.se

This article is copyrighted as indicated in the article. Reuse of AIP content is subject to the terms at: http://scitation.aip.org/termsconditions. Downloaded to IP: 77.238.32.12 On: Tue, 14 Oct 2014 12:41:39

$$F_{\rm EL} = \frac{1}{2}C'(t)\left[2V_{\rm CPD}V_{\rm AC}\cos(\omega_{\rm E}t+\phi_{\rm E}) + \frac{1}{2}V_{\rm AC}^2\cos(2\omega_{\rm E}t+2\phi_{\rm E}) + \frac{V_{\rm AC}^2}{2} + V_{\rm CPD}^2\right]. \quad (6)$$

Re-arranging terms, it is possible to separate the electrostatic force in components at different frequencies ω_i with complex amplitudes $\hat{F}_{\omega_i}$

$$\hat{F}_{\rm DC} = \frac{1}{2}a_0\left(\frac{V_{\rm AC}^2}{2}+V_{\rm CPD}^2\right), \quad (7a)$$

$$\hat{F}_{\omega_{\rm D}} = \frac{1}{2}a_1\left(\frac{V_{\rm AC}^2}{2}+V_{\rm CPD}^2\right)e^{i\phi_{\rm D}}, \quad (7b)$$

$$\hat{F}_{\omega_{\rm E}} = a_0V_{\rm CPD}V_{\rm AC}e^{i\phi_{\rm E}}, \quad (7c)$$

$$\hat{F}_{2\omega_{\rm E}} = \frac{1}{4}a_0V_{\rm AC}^2e^{i2\phi_{\rm E}}, \quad (7d)$$

$$\hat{F}_{\omega_{\rm D}\pm\omega_{\rm E}} = \frac{1}{2}a_1V_{\rm CPD}V_{\rm AC}e^{i\phi_{\rm D}}e^{\pm i\phi_{\rm E}}, \quad (7e)$$

$$\hat{F}_{\omega_{\rm D}\pm2\omega_{\rm E}} = \frac{1}{8}a_1V_{\rm AC}^2e^{i\phi_{\rm D}}e^{\pm i2\phi_{\rm E}}. \quad (7f)$$

Other force components are present at frequencies $k\omega_{\rm D}$, $k\omega_{\rm D}\pm\omega_{\rm E}$ and $k\omega_{\rm D}\pm2\omega_{\rm E}$. However, in this analysis we limit ourselves to the components at low frequency and around the cantilever drive frequency since they are the ones experimentally detectable with good signal-to-noise ratio.

With the driving scheme used in ImEFM, it is possible to extract $V_{\rm CPD}$ from the measurement of the force components at low frequency (7c)–(7d)

$$V_{\rm CPD} = \frac{V_{\rm AC}}{4}\frac{\hat{F}_{\omega_{\rm E}}}{\hat{F}_{2\omega_{\rm E}}}e^{i\phi_{\rm E}} \quad (8)$$

or from the components at high frequency (7e)–(7f)

$$V_{\rm CPD} = \frac{V_{\rm AC}}{4}\frac{\hat{F}_{\omega_{\rm D}\pm\omega_{\rm E}}}{\hat{F}_{\omega_{\rm D}\pm2\omega_{\rm E}}}e^{\pm i\phi_{\rm E}}. \quad (9)$$

The phase factor $\phi_{\rm E}$ can be set to zero by ensuring that the AC voltage is in phase with the lock-in reference signal.

Obtaining $V_{\rm CPD}$ from Eq. (8) or from Eq. (9) is in principle equivalent; however, in experimental conditions noise is present in the detection system and the cantilever resonance allows for a measurement of the force components (7e) and (7f) with much higher signal-to-noise ratio, limited in sensitivity only by the thermal noise force. Note that $V_{\rm CPD}$ depends on a measurement of force, which is obtained from the cantilever motion by a calibration procedure.[9,10] However in ImEFM, $V_{\rm CPD}$ is proportional to the ratio of two forces. Thus, only the frequency dependence of the cantilever transfer function (resonance frequency and quality factor) is significant to the calibration, while the mode stiffness and the optical lever responsivity fall out of the ratio.

The expressions for the contact potential difference hold for any form of the capacitance gradient since we did not truncate the polynomial expansion (4) to a finite order. In particular, the validity of the technique does not depend upon the assumption that the capacitance gradient, or its first derivative, is constant in the oscillation range.[11] Under the condition of low drive amplitude, it is, however, possible to approximate the capacitance gradient as a linear function of z, i.e., truncate expansion (4) at $n=1$. Equation (5) gives $a_0 = C'$ and $a_1 = A_{\rm D}C''$, and it is possible to evaluate the capacitance gradient and its first derivative at h from the measured force components

$$C' = 4\frac{\hat{F}_{2\omega_{\rm E}}}{V_{\rm AC}^2}e^{-i2\phi_{\rm E}}, \quad (10a)$$

$$C'' = 8\frac{\hat{F}_{\omega_{\rm D}\pm2\omega_{\rm E}}}{A_{\rm D}V_{\rm AC}^2}e^{-i\phi_{\rm D}}e^{\mp i2\phi_{\rm E}}. \quad (10b)$$

We simulated ImEFM by numerically integrating the differential equation that models the cantilever dynamics

$$\ddot{d} + \frac{\omega_0}{Q}\dot{d} + \omega_0^2 d = \frac{\omega_0^2}{k}F_{\rm TOT}(t,z), \quad (11)$$

where $d = z - h$ is the cantilever deflection, z is the tip-sample distance, h is the tip resting position, and ω_0, Q, and k are the resonance frequency, quality factor, and stiffness of the first flexural mode of the cantilever. The total force on the cantilever $F_{\rm TOT}$ is given by three contributions: a sinusoidal drive force close to the first flexural resonance due to the inertial actuation, the electrostatic force for an axial symmetric electrode over an infinite plane surface,[8] and the tip-surface force modelled by a Lennard-Jones potential.[12] The result of the numerical integration is the cantilever deflection signal as a function of time. We compute the Discrete Fourier Transform to obtain the frequency spectrum of cantilever deflection $\hat{d}(\omega)$, from which we then calculate the force spectrum $\hat{F}(\omega)$ by multiplying with the cantilever inverse response function $\hat{\chi}^{-1}$

$$\hat{F}(\omega) = \hat{\chi}^{-1}\hat{d}(\omega), \quad (12a)$$

$$\hat{\chi}^{-1}(\omega) = k\left(1 + i\frac{\omega}{\omega_0 Q} - \frac{\omega^2}{\omega_0^2}\right). \quad (12b)$$

We finally calculate $V_{\rm CPD}$ according to Eqs. (8) and (9).

From the results of the simulation, it is possible to investigate the validity of assumption (3). When the probe softly interacts with the sample the motion is prevalently harmonic, i.e., the amplitude component at the drive frequency is higher than any other component by two or more orders of magnitude. The numerical integrator can compute all the intermodulation products, however, when a realistic detector noise level is added to the simulation, only two intermodulation products are visible above the noise on each side of the drive frequency. On the other hand, when the interaction with the surface is stronger more peaks arise above the noise level and the reconstruction of the $V_{\rm CPD}$ is not accurate.

By simulating the cantilever dynamics, we investigate the effect of the electrostatic force and the tip-surface force (modelled by a Lennard-Jones potential) separately. The simulations confirm that it is the non-linear electrostatic force that up-converts the electrostatic frequency to the first flexural resonance. The short range tip-surface force is not required to measure the intermodulation spectrum.

This article is copyrighted as indicated in the article. Reuse of AIP content is subject to the terms at: http://scitation.aip.org/termsconditions. Downloaded to IP: 77.238.32.12 On: Tue, 14 Oct 2014 12:41:39

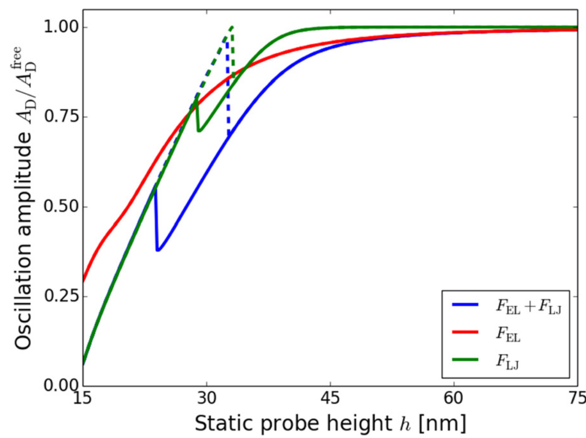

FIG. 1. Simulated cantilever oscillation amplitude at the mechanical drive frequency as a function of distance from the sample during approach (solid line) and retract (dashed line) with initial amplitude $A_D^{free} = 20$ nm. The AC electrostatic force causes the amplitude to drop faster than in the case with short-range forces only. Hysteresis is visible in the approach-retract curves with short-range interactions.

Moreover, Fig. 1 shows that by adding the AC electrostatic force to the tip-surface interaction, more frequency components are available to accommodate the oscillation energy of the cantilever, causing the oscillation amplitude to drop at larger distance from the surface and thus giving a more stable feed-back in the so-called non-contact regime where attractive forces dominate over repulsive forces. It is in this regime that our single pass scan is performed, corresponding to a static probe height $h \approx 60$ nm (for a free oscillation amplitude $A_D = 30$ nm and an amplitude set-point of 90%).

Experiments were performed on a JPK NanoWizard 3 AFM mounted on an inverted optical microscope. The generation of the electrical and mechanical drive signals and the acquisition of the intermodulation spectra were performed with an intermodulation lock-in analyser.[13] To experimentally validate the technique, we applied a series of DC potential steps with different amplitudes while performing ImEFM on a gold substrate (Fig. 2(b)). We used a Cr-Au coated cantilever by Mikromash with 300.5 kHz resonance frequency, driven close to resonance with a free oscillation amplitude of 35 nm. We applied a 6 V AC potential at 469 Hz with a pixel time of 2.1 ms. The technique was able

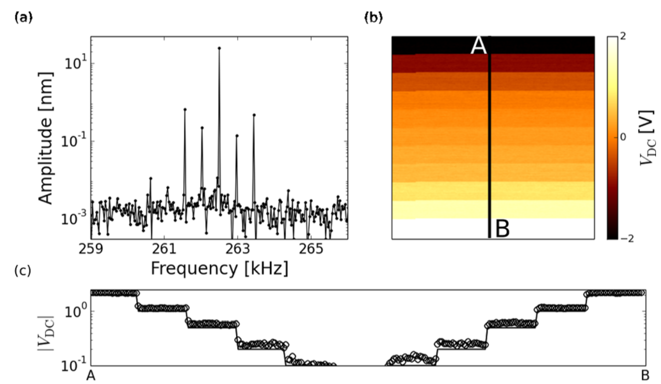

FIG. 2. Typical intermodulation spectrum around resonance when performing ImEFM (a). As the cantilever scans over a gold surface (b), different steps of DC potential are applied to the sample ((c), solid line). ImEFM is able to measure the correct variation in surface potential.

to measure the intermodulation spectrum (Fig. 2(a)) and reconstruct the potential applied to the sample within a few % and with very low noise (Fig. 2(c)).

We apply the technique to spatially resolve the photo-generation of charge in a TQ1:PCBM:C60 (Refs. 14–16) thin film spin-coated on an ITO electrode. We acquire two V_{CPD} images, one in dark and one under illumination, during the scan trace and re-trace, respectively. We then calculate the surface photo-voltage V_{SPV} as the difference of the trace and re-trace V_{CPD} images.[17] Fig. 3 highlights the presence of domains with size of the order of 50 nm, and we notice a correlation between areas of low work function (low V_{CPD} in the dark), and areas of high surface photo-voltage. Areas with high values of V_{SPV} correspond to an increased V_{CPD} under illumination, which can be explained by a higher concentration of photo-generated holes than electrons, and therefore a region with a high concentration of donors (lower work function).

We demonstrated an EFM technique for mapping surface potential with high signal-to-noise ratio, making use of the high force sensitivity of the cantilever mechanical resonance and frequency mixing due to the nonlinear capacitance gradient. Being an open-loop technique, the feed-back induced cross talk is avoided and the measurement speed is not limited by the feed-back bandwidth. The absence of an applied DC bias makes this technique good for

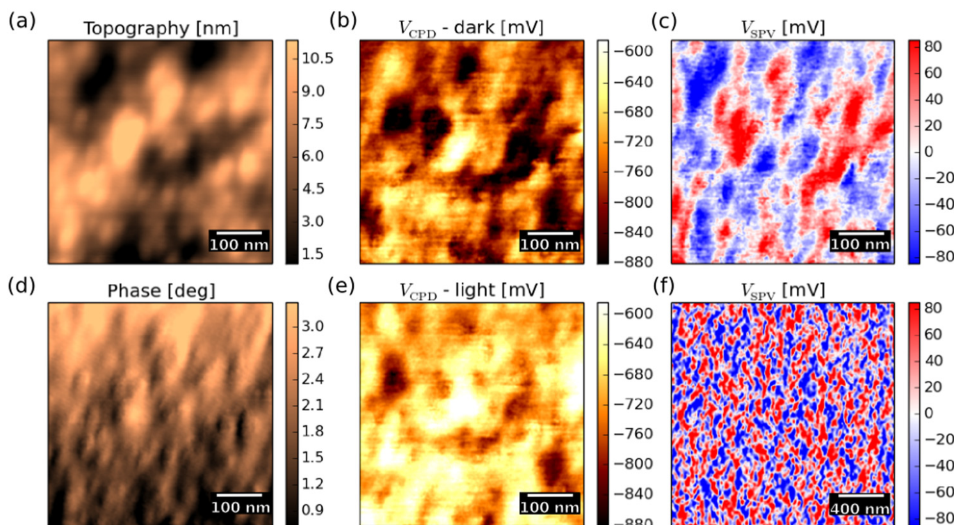

FIG. 3. (a)–(e) ImEFM on a TQ1:PCBM:C60 sample, 500 nm scan size with 256 × 256 pixels resolution. The total acquisition time is 5 min. Despite the very flat topography and limited contrast in the phase image, different domains are clearly visible in the contact potential difference images in dark and under illumination, and especially in the surface photo-voltage image, which shows domains with size of order 50–100 nm. The domains appear to be regular across the surface as shown with a bigger scan size of 2 μm (f).

This article is copyrighted as indicated in the article. Reuse of AIP content is subject to the terms at: http://scitation.aip.org/termsconditions. Downloaded to IP: 77.238.32.12 On: Tue, 14 Oct 2014 12:41:39

characterising bias sensitive systems and materials with high work function that would require additional voltage amplifiers with feed-back based techniques. Finally, the ability to perform a single-pass measurement significantly lowers the imaging time and provides higher lateral resolution than interleaved lift-mode techniques.

The authors acknowledge financial support from the Swedish Research Council (VR), the Knut and Alice Wallenberg Foundation, and the Olle Engkvist Foundation. We are grateful for fruitful discussions with Liam Collins.

[1]M. Nonnenmacher, M. P. OBoyle, and H. K. Wickramasinghe, Appl. Phys. Lett. **58**, 2921 (1991).
[2]M. J. Cadena, R. Misiego, K. C. Smith, A. Avila, B. Pipes, R. Reifenberger, and A. Raman, Nanotechnology **24**, 135706 (2013).
[3]H. Hoppe, T. Glatzel, M. Niggemann, A. Hinsch, M. C. Lux-Steiner, and N. S. Sariciftci, Nano Lett. **5**, 269 (2005).
[4]L. Collins, J. I. Kilpatrick, S. A. L. Weber, A. Tselev, I. V. Vlassiouk, I. N. Ivanov, S. Jesse, S. V. Kalinin, and B. J. Rodriguez, Nanotechnology **24**, 475702 (2013).
[5]O. Takeuchi, Y. Ohrai, S. Yoshida, and H. Shigekawa, Jpn. J. Appl. Phys., Part 1 **46**, 5626 (2007).
[6]N. Kobayashi, H. Asakawa, and T. Fukuma, J. Appl. Phys. **110**, 044315 (2011).
[7]L. Collins, J. I. Kilpatrick, M. Bhaskaran, S. Sriram, S. A. L. Weber, S. P. Jarvis, and B. J. Rodriguez, in *Proceedings of ISAF-ECAPD-PFM 2012* (IEEE, 2012), pp. 1–4.
[8]S. Hudlet, M. Saint Jean, C. Guthmann, and J. Berger, Eur. Phys. J. B **2**, 5 (1998).
[9]J. Sader, J. Chon, and P. Mulvaney, Rev. Sci. Instrum. **70**, 3967 (1999).
[10]M. J. Higgins, R. Proksch, J. E. Sader, M. Polcik, S. Mc Endoo, J. P. Cleveland, and S. P. Jarvis, Rev. Sci. Instrum. **77**, 013701 (2006).
[11]C. Maragliano, A. Glia, M. Stefancich, and M. Chiesa, J. Appl. Phys. **115**, 124311 (2014).
[12]J. Melcher, D. Kiracofe, S. Hu, S. D. Johnson, S. Balasubramaniam, and A. Raman, *Veda Manual* (2012), available at https://nanohub.org/resources/14934.
[13]E. A. Tholén, D. Platz, D. Forchheimer, V. Schuler, M. O. Tholén, C. Hutter, and D. B. Haviland, Rev. Sci. Instrum. **82**, 026109 (2011).
[14]C. Lindqvist, J. Bergqvist, C.-C. Feng, S. Gustafsson, O. Bäcke, N. D. Treat, C. Bounioux, P. Henriksson, R. Kroon, E. Wang, A. Sanz-Velasco, P. M. Kristiansen, N. Stingelin, E. Olsson, O. Inganäs, M. R. Andersson, and C. Müller, Adv. Energy Mater. **4**, 1301437 (2014).
[15]C. Lindqvist, J. Bergqvist, O. Bäcke, S. Gustafsson, E. Wang, E. Olsson, O. Inganäs, M. R. Andersson, and C. Müller, Appl. Phys. Lett. **104**, 153301 (2014).
[16]A. Diaz de Zerio Mendaza, J. Bergqvist, O. Bäcke, C. Lindqvist, R. Kroon, F. Gao, M. R. Andersson, E. Olsson, O. Inganäs, and C. Müller, J. Mater. Chem. A **2**, 14354 (2014).
[17]E. J. Spadafora, R. Demadrille, B. Ratier, and B. Grévin, Nano Lett. **10**, 3337 (2010).

This article is copyrighted as indicated in the article. Reuse of AIP content is subject to the terms at: http://scitation.aip.org/termsconditions. Downloaded to IP: 77.238.32.12 On: Tue, 14 Oct 2014 12:41:39